Nitrogen Quadrupole Hyperfine Structure in the Rotational Spectrum of 2-, 3-, and 4-Fluoro-Benzonitrile. A Comparative High Resolution Microwave Fourier Transform Study

Olaf Böttcher and Dieter H. Sutter

Abteilung Chemische Physik im Institut für Physikalische Chemie
der Christian Albrechts Universität zu Kiel

Z. Naturforsch. **43a**, 47–58 (1988); received October 14, 1987

A microwave Fourier transform study of the rotational spectrum of 3-fluoro-benzonitrile was carried out to study the ^{14}N quadrupole coupling and to give improved rotational constants and centrifugal distortion parameters. In order to fully exploit the high resolution inherent to the experimental technique, frequencies, linewidths, intensities and phases were directly fitted to the observed transient emission signals. The quadrupole coupling constants are discussed in comparison to those of the related molecules 2-fluoro-benzonitrile, 4-fluoro-benzonitrile, and benzonitrile itself. For this comparison a sufficient number of hfs-patterns of the latter molecules was remeasured to derive coupling constants of comparable reliability. The four molecules may be grouped into two pairs. In benzonitrile and in 3-fluoro-benzonitrile the CN-bond shows a smaller deviation from cylindrical symmetry than in 2- and 4-fluoro-benzonitrile.

In view of our current interest in substituent effects in small aromatic molecules, we started a high resolution study of the rotational spectrum of 3-fluoro-benzonitrile. In an earlier investigation [1, 2] we had been able to show that fluorine substitution has a significant position dependent effect on the ring current properties of benzenes and pyridines. In the present investigation we wanted to check whether such a position-dependence of the interaction of the substituent with the ring system would also show up as an alternation in the in-plane and out-of-plane p-electron densities at the nitrile nitrogen atom as probed by the nuclear quadrupole hyperfine interaction. For small non-aromatic molecules Cox, Dreizler and coworkers [3] have argued, that the nitrile group has cylindrical symmetry. For the aromatic benzonitriles however, we expected to find a difference between the in-plane and out-of-plane nitrogen p-densities with a significant and position dependent effect on fluorine substitution.

Reprint requests to Prof. Dr. Dieter H. Sutter, Institut für Physikalische Chemie der Christian Albrechts Universität zu Kiel, Olshausenstraße 40, D-2300 Kiel, West Germany.

Experimental Details

The sample, a colourless liquid at room temperature, was purchased from Aldrich Chemie, Steinheim, West Germany (purity > 98%), and was used after several bulb to bulb distillations without further purification. The microwave spectrum, previously assigned in a low resolution study by Dutta et al. [4], who did not resolve the nitrogen hyperfine structure, was measured using the microwave Fourier transform spectrometer developed by H. Dreizler and coworkers [5–8]. Typical sample pressures in the waveguide cell were below 1 mTorr and the cell temperatures ranged between $-20\,^{\circ}C$ and $-40\,^{\circ}C$. Rapidly decreasing saturation pressure precluded cooling to lower temperatures.

In Fig. 1 we show the orientation of the principal inertia axes system within the molecule. With electric dipole moment components of $\mu_a \approx 1.5$ Debye and $\mu_b \approx 2.7$ Debye, as estimated from the known dipole moments of fluorobenzene and benzonitrile with the modified vector addition model described in [9], the rotational spectrum consists of stronger b-type transitions and weaker a-type transitions. It is rather dense. In order to give an impression of the typical resolution and signal-to-noise ratio obtained in the present in-

0932-0784 / 88 / 0100-0047 $ 01.30/0. – Please order a reprint rather than making your own copy.

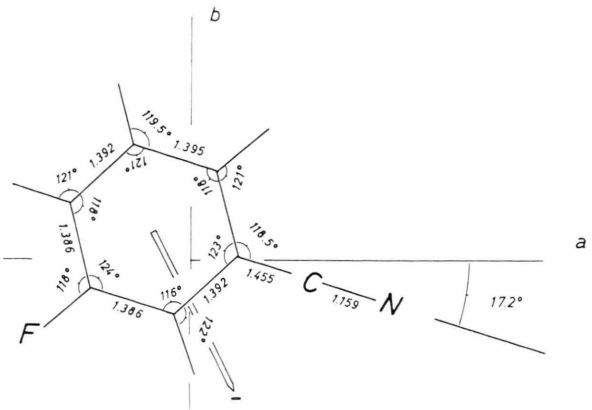

Fig. 1. Orientation of the principal inertia axes system and of the molecular electric dipole moment vector in meta-fluoro-benzonitrile. Since the equilibrium structure is not yet known, we used a blend of the known structures of fluorobenzene (34) and benzonitrile (35) which is in fair agreement with the observed rotational constants. The dipole moment is estimated (9) as 85% of the vector sum of the experimental dipole moments of benzonitrile (36) and of fluorobenzene (37).

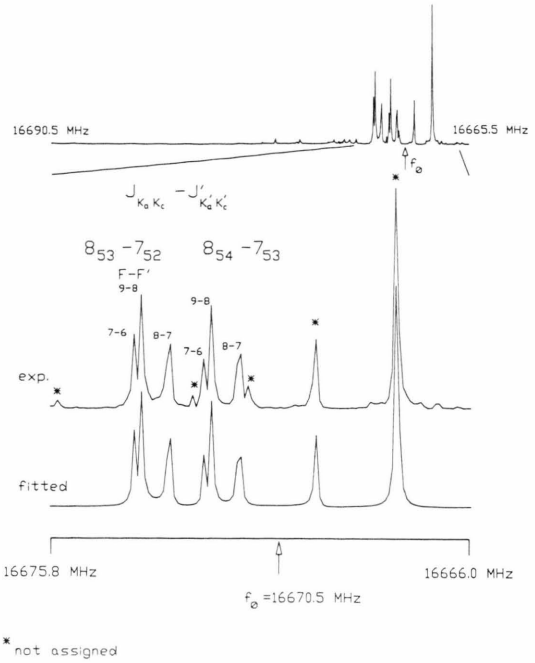

Fig. 2. Power spectra of the $K_a = 5$ K-doublet $8_{53} - 7_{52}$ and $8_{54} - 7_{53}$ of meta-fluoro-benzonitrile. The experimental conditions were: pressure 1 mTorr, temperature 238 K, polarizing frequency 16 670.5 MHz, duration of the exciting pulse 100 nsec, delay time between the end of the polarizing pulse and the start of sampling approximately 2.8 μsec. 5760 k decays, each with 1024 data points taken with a sampling interval of 20 nsec were averaged before data processing. – The upper trace shows the traditional power spectrum of a 25 MHz range. The second trace shows an enlarged part of the same spectrum. The peak frequencies and amplitudes corresponding to this power spectrum are then used as input data for the decay-fit routine described in the text. The lower trace shows the power spectrum corresponding to the eight strongest transient emission signals present in the decay. For a final analysis one has to check the power spectrum of the residuum, e.g. the difference between the experimental decay and the optimized decay resulting from the fit of a limited number of emission signals (here eight). Hitherto hidden spectral features, which might spoil the quality of the frequency determinations and which must be included in the fit may shown up. (In our example the optimized emission frequencies of two satellites are still about 10 kHz off if only 8 signals are fitted).

vestigation, we show the power spectra [10] of an a-type K-doublet close to 16.7 GHz in Figure 2.

Determination of the Resonance Frequencies and Analysis of the Spectrum

As we have pointed out earlier [11], power spectra (for an example see Fig. 2), although excellent to give a first impression of the spectrum, should not be used to fit molecular parameters such as for instance the nuclear quadrupole coupling constants, because their peak frequencies can be shifted considerably with respect to the resonance frequencies. This is true even in the case of apparently well resolved lines. In closely spaced multiplets satellites may even vanish, depending on the experimental conditions. This problem is discussed in more detail in the appendix. For the frequency determinations we therefore used a decay fit routine developed at Kiel by J. Haekel, in which the frequencies, amplitudes, relaxation times and phases of the transient molecular emissions are fitted directly to the experimental decays by a least squares procedure. Details of the procedure will be described by Haekel et al. in a separate publication.

In total 105 different rotational transitions with J-values between 5 and 30 were measured. More than half of them showed a well resolved ^{14}N quadrupole hyperfine structure. In Table 1 we give a small part of the frequencies obtained. The complete listing is deposited under registration number TNA 12 at the university library at Kiel and is available upon request [12].

The analysis of the recorded transitions was carried out in an iterative treatment of the centrifugally distorted rotor [13] and the ^{14}N quadrupole hyperfine

Table 1. Part of the recorded rotational transitions of meta-fluoro-benzonitrile. The frequencies are given in MHz. ν_{center} are the hypothetical center frequencies of the corresponding complete hfs pattern. $\Delta\nu_{exp}$ are the measured splittings, to which the quadrupole coupling constants were fitted. $\Delta\nu_{calc}$ are the splittings calculated from the optimized rotational constants (Table 2) and quadrupole coupling constants (Table 3) according to (1). ν_{exp} are the experimental frequencies of the hfs components. They were obtained from the observed transient emission signals by the decay-fit routine described in the text.

$J_{K_a K_c} - J'_{K'_a K'_c}$	$F - F'$	ν_{exp}	$\Delta\nu_{exp}$	$\Delta\nu_{calc}$	ν_{center}
5 4 2 – 5 3 3	6 6	16422.984	−0.889	−0.890	16423.224
	5 5	16423.873	0.713	0.710	
	4 4	16422.808			
5 2 4 – 4 1 3	6 5	15850.302	−0.248	−0.254	15850.364
	5 4	15850.550	0.358	0.360	
	4 3	15850.192			
6 3 3 – 5 3 2	7 5	12609.791	0.337	0.334	12609.685
	6 5	12609.454	−0.383	−0.386	
	5 4	12609.837			
6 4 2 – 6 3 3	7 7	16259.850	−0.650	−0.647	16260.041
	6 6	16260.500	0.750	0.755	
	5 5	16259.750			
6 4 3 – 6 3 4	7 7	16405.558	−0.644	−0.642	16405.743
	6 6	16406.202	0.752	0.750	
	5 5	16405.450			
6 2 5 – 5 1 4	7 6	17163.111	−0.175	−0.177	17163.156
	6 5	17163.286	0.250	0.246	
	5 4	17163.036			
7 6 1 – 6 6 0	8 7	14542.140	0.824	0.817	14541.910
(7 6 2 – 6 6 1)	7 6	14541.316	−0.988	−0.985	
	6 5	14542.304			
7 4 3 – 6 4 2	8 7	14614.062	0.368	0.370	14613.957
	7 6	14613.698	−0.431	−0.427	
	6 5	14614.129			
7 5 2 – 6 5 1*	8 7	14564.879	0.551	0.570	14564.721
	7 6	14564.328	−0.670	−0.677	
	6 5	14564.998			
7 5 3 – 6 5 2*	8 7	14564.663	0.571	0.570	14564.500
	7 6	14564.092	−0.669	−0.677	
	6 5	14564.761			
7 4 4 – 6 4 3	8 7	14603.039	0.363	0.369	14602.928
	7 6	14602.676	−0.425	−0.427	
	6 5	14603.101			
7 4 3 – 7 3 4	8 8	16054.068	−0.490	−0.492	16054.203
	7 7	16054.558	0.560	0.561	
	6 6	16053.998			
7 4 4 – 7 3 5	8 8	16401.979	−0.488	−0.484	16402.137
	7 7	16402.467	0.559	0.554	
	6 6	16401.908			
7 3 5 – 7 2 6	8 8	12660.988	−0.350	−0.344	12661.094
	7 7	12661.338	0.394	0.394	
	6 6	12660.943			
8 6 2 – 7 6 1	9 8	16636.775	0.553	0.552	16636.612
(8 6 3 – 7 6 2)	8 7	16636.222	−0.643	−0.642	
	7 6	16636.865			
8 7 1 – 7 7 0	9 8	16616.819	0.747	0.747	16616.604
(8 7 2 – 7 7 1)	8 7	16616.072	−0.879	0.879	
	7 6	16616.951			
8 5 3 – 7 5 2	9 8	16671.227	0.387	0.386	16671.113
	8 7	16670.840	−0.446	−0.443	
	7 6	16671.286			
8 5 4 – 7 5 3	9 8	16670.302	0.387	0.386	16670.191
	8 7	16669.915	−0.447	−0.443	
	7 6	16670.362			
8 4 4 – 8 3 5	9 9	15715.436	−0.386	−0.388	15715.516
	8 8	15715.822	0.439	0.437	
	7 7	15715.375			

* not included in the hfs-fit

interaction [14]. In the first step of the cycle, the ^{14}N quadrupole constants χ_{aa}, χ_{bb}, and χ_{cc} were fitted to the observed hfs-splittings of the rotational transitions (see Fig. 2 and Table 1). Since in our case the hyperfine splitting of the rotational levels is small as compared to the rotational energy differences, the standard first order energy expression for an effective rigid rotor containing one quadrupole nucleus [15] was used in this step. It is given by

$$W_{J,K_aK_c,I,F} = A\langle\hat{J}_a^2\rangle + B\langle\hat{J}_b^2\rangle + C\langle\hat{J}_c^2\rangle + \frac{[3C_F(C_F+1)/4 - I(I+1)J(J+1)]}{I(2I-1)J(2J-1)(J+1)(2J+3)} \cdot (\chi_{aa}\langle\hat{J}_a^2\rangle + \chi_{bb}\langle\hat{J}_b^2\rangle + \chi_{cc}\langle\hat{J}_c^2\rangle). \quad (1)$$

A, B, C = rotational constants ($A \geq B \geq C$).

$\langle\hat{J}_a^2\rangle$ = $\langle J, K_a K_c|\hat{J}_a^2|J, K_a K_c\rangle$ = asymmetric top expectation value of the square of the angular momentum operator around the a-axis of the molecular principal inertia axes system as measured in units of $\hbar^2$ (and cyclic permutations).

I, J = quantum numbers of ^{14}N nuclear spin and molecular overall rotation, respectively.

C_F = $F(F+1) - I(I+1) - J(J+1)$ with F the quantum number of the total angular momentum due to ^{14}N-spin and overall rotation. ($\boldsymbol{F} = \boldsymbol{I} + \boldsymbol{J}$). For each rotational state with given J, F runs from $|I-J|$ to $I+J$ in steps of one.

χ_{aa} = $eV_{aa}Q/h$ = nuclear quadrupole coupling constant (and cyclic permutations $a \rightarrow b \rightarrow c \rightarrow a$).

e = proton charge.

Q = nuclear quadrupole moment of the ^{14}N nucleus. ($Q = 0.01 \cdot 10^{-24}$ cm^2 [16]).

h = Planck's constant.

V_{aa} = vibronic ground state expectation value for the second derivative of the intramolecular Coulomb potential with respect to a, taken at the position of the ^{14}N nucleus.

In this step approximate rotational constants were used to calculate the asymmetric top expectation values $\langle\hat{J}_a^2\rangle$, etc. The quadrupole coupling constants, fitted to the observed splittings, were then used to reconstruct the center frequencies of each observed hfs multiplet [17] from the measured frequencies of its most intense satellites.

In the second step of the cycle, improved rotational constants and quartic centrifugal distortion constants were fitted to these center frequencies. Watsons S-reduction of the effective rotational Hamiltonian in the I^r representation was used in this step:

$$\hat{\mathscr{H}}/h = A\hat{J}_a^2 + B\hat{J}_b^2 + C\hat{J}_c^2 - D_J\hat{J}^4 - D_{JK}\hat{J}^2\hat{J}_a^2 - D_k\hat{J}_a^4 + d_1\hat{J}^2(\hat{J}_+^2 + \hat{J}_-^2) + d_2(\hat{J}_+^4 + \hat{J}_-^4)$$

with $\hat{J}_+ = \hat{J}_b + i\hat{J}_c$ and $\hat{J}_- = \hat{J}_b - i\hat{J}_c$, and the centrifugal distortion constants D_J, $D_{JK}D_K$, d_1 and d_2.

This least squares fit of the rotational constants and the centrifugal distortion constants completes the cycle.

Then the resulting improved rotational constants A, B, and C were used as input data for "step one" of a new iteration cycle. This iterative procedure became stable within the roundoff errors after 3 cycles. Our final rotational constants and centrifugal distortion constants are given in Table 2. In Table 3 we give our quadrupole coupling constants. Also given for later comparison are the corresponding values for the related molecules ortho- and para-fluoro-benzonitrile and for benzonitrile itself. These values differ from those published earlier [20–22], since, in order to be able to compare them with data of the same high reliability, we have remeasured and reanalyzed several low-J-transitions for both fluoro-benzonitriles with the method outlined above (see Tables 4 and 5). Similarly the improved values for benzonitrile itself were determined recently in our group by Vormann [23].

The superiority of the decay fit procedure used here as compared to the traditional analysis of the power spectra of the transient emission signals is obvious from Table 3. With essentially the same signal to noise quality in the observed decays, the least squares standard deviations of the optimized quadrupole coupling constants have dropped considerably.

Comparison of the Quadrupole Coupling Constants

The experimental results presented in Table 3 show that the local electronic environment of the nitrogen nucleus indeed lacks cylindrical symmetry around the CN-axis. Para-fluoro-benzonitrile is more asymmetric than benzonitrile and ortho-fluoro-benzonitrile is more asymmetric than meta-fluoro-benzonitrile. As will be shown in the following, these differences can be

Table 2. Rotational constants in MHz and quartic centrifugal distortion constants in kHz fitted to the hfs center frequencies of 105 rotational transitions involving J-values between 5 and 30. The effective rotational Hamiltonian used here is given in (2) of the text. Single standard deviations of the fit (in brackets) are given in units of the least significant digit. Note that d_1 and d_2 are closely correlated. V. Typkes program ZFAP4 [19] was used for this analysis.

		Correlation coefficient matrix							
A	3388.61073 (35) MHz	1.00							
B	1186.63868 (13) MHz	0.78	1.00						
C	878.69740 (10) MHz	0.49	0.48	1.00					
D_J	0.0334 (5) kHz	0.63	0.75	0.40	1.00				
D_{JK}	0.0443 (19) kHz	0.62	0.72	−0.03	0.77	1.00			
D_K	1.2179 (6) kHz	0.26	−0.11	0.34	0.10	−0.33	1.00		
d_1	−0.0135 (2) kHz	−0.39	−0.62	0.28	−0.47	−0.87	0.53	1.00	
d_2	−0.0031 (1) kHz	0.31	0.54	−0.29	0.36	0.79	−0.55	0.98	1.00
		A	B	C	D_J	D_{JK}	D_K	d_1	d_2

Table 3. Experimental ^{14}N quadrupole coupling constants (in MHz) for meta-fluoro-benzonitrile (second column). Also given are our improved quadrupole coupling constants for ortho- and para-fluoro-benzonitrile and the redetermined coupling constants of benzonitrile itself [23]. The older values are given in brackets (see text for the discrepancies). For better comparison, the coupling tensors of ortho- and meta-fluoro-benzonitrile have been transformed into a coordinate system aligned to the CN bond (x-axis) with its z-axis perpendicular to the molecular plane (see text). The quoted uncertainties in the χ_{xx} and χ_{yy}-values reflect $a \pm 1°$ uncertainty assumed for the angle θ between the molecular a-axis and the x-axis. The uncertainties given for the experimental coupling constants χ_{aa}, χ_{bb}, and χ_{cc} are single deviations of the least squares fit to the observed hfs-splittings. G. E. Herberichs program HT1NQ was used for this analysis [18].

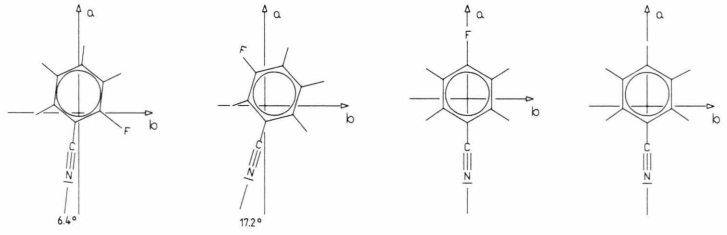

χ_{aa}	−4.147 (7)	−3.682 (5)	−4.233 (5)	−4.224 (4)
	(−4.239 (63))		(−4.198 (7))	(−4.187 (70))
χ_{bb}	2.223 (6)	1.696 (4)	2.337 (6)	2.290 (3)
	(2.338 (152))		(2.395 (12))	(2.301 (80))
χ_{cc}	1.924 (6)	1.986 (4)	1.897 (6)	1.954 (3)
	(1.901 (152))		(1.803 (12))	(1.886 (80))
χ_{xx}	−4.228 (26)	−4.252 (78)	−4.233	−4.244
χ_{yy}	2.304 (26)	2.266 (78)	2.337	2.290
χ_{zz}	1.924	1.986	1.897	1.954
$(\chi_{yy} - \chi_{zz})$	0.380 (26)	0.280 (78)	0.440	0.336

rationalized within the simple model of valence bond resonance structures, while a much more sophisticated CNDO/2 calculation fails.

The quadrupole coupling constants are directly related to the vibronic groundstate expectation value of the second derivatives V_{aa}, V_{bb}, and V_{cc}, of the intramolecular Coulomb potential at the ^{14}N nucleus. Within the Born-Oppenheimer approximation they may be written as

$$\chi_{aa} = (e\,Q/h) \cdot \langle v = 0 | \langle n = 0 \left| \sum_i e_i \frac{3\,a_{iN}^2 - r_{iN}^2}{r_{iN}^5} \right| n = 0 \rangle | v = 0 \rangle \quad (3)$$

(and cyclic permutations).

Table 4. ^{14}N hfs multiplets of para-fluoro-benzonitrile. To obtain the satellite frequencies, the recorded transient emission signals were subjected to the decay-fit procedure described in the text. The coupling constants reported in Table 3 were fitted to these splittings. For the abbreviations see Table 1. (The frequencies are given in MHz).

$J_{K_a K_c} - J'_{K'_a K'_c}$	$F - F'$	ν_{exp}	$\Delta\nu_{exp}$	$\Delta\nu_{calc}$	ν_{center}
5 4 1 – 4 4 0	6 – 5	9015.007			9014.721
(5 4 2 – 4 4 1)	5 – 4	9013.867	1140	1142	
	4 – 3	9015.353	−1486	−1483	
5 2 3 – 4 2 2	6 – 5	9064.988			9064.896
	5 – 4	9064.687	309	309	
	4 – 3	9065.020	− 341	− 338	
5 1 5 – 4 1 4	6 – 5	8635.560			8635.524
	5 – 4	8635.470	90	88	
	4 – 3	8635.516	− 46	− 46	
6 4 2 – 5 4 1	7 – 6	10820.226			10820.044
(6 4 3 – 5 4 2)	6 – 5	10819.558	668	668	
	5 – 4	10820.368	− 810	− 812	
6 5 1 – 5 5 0	7 – 6	10817.352			10817.092
(6 5 2 – 5 5 1)	6 – 5	10816.325	1027	1026	
	5 – 4	10817.615	−1277	−1275	
12 1 11 – 12 1 12	13 – 13				10950.866
	11 – 11	10950.905	147	147	
	12 – 12	10950.758			

$|v = 0\rangle$ = vibrational ground state function. Here v stands for all 33 vibrational quantum numbers of meta-fluoro-benzonitrile.

$|n = 0\rangle$ = electronic "fixed nuclei" ground state function. It depends parametrically on the coordinates of the nuclei.

e_i = Coulomb charge of the i-th particle outside the ^{14}N nucleus. ($-e$ for electrons, $+Z_n e$ for the n-th nucleus with Z_n its atomic number).

a_{iN} = $a_i - a_N$ = differences in the a-coordinates of charge e_i and of the nitrogen nucleus, where the second derivative is calculated.

r^2_{iN} = $(a_i - a_N)^2 + (b_i - b_N)^2 + (c_i - c_N)^2$.

Due to the r^2_{iN} dependence, the χ_{gg} values ($g = a, b, c$) are predominantly determined by the immediate electronic environment of the quadrupole nucleus, and a simplified LCAO-MO-treatment [24] leads to the following approximate expression for their values:

$$\chi_{aa} = (e\, q_{210}\, Q/h) \cdot [P_{aa} - (P_{bb} + P_{cc})/2]. \qquad (4)$$

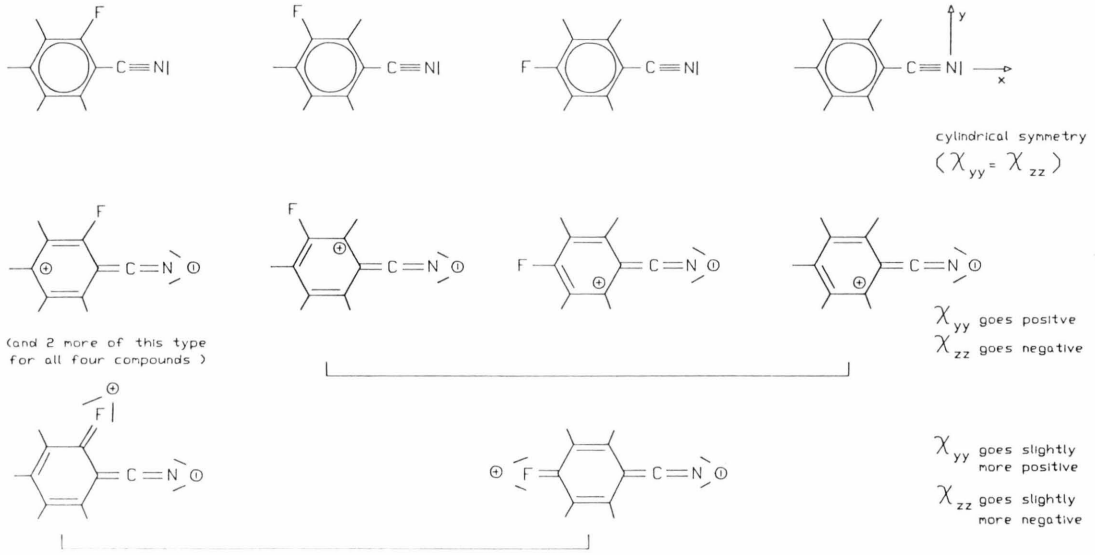

Fig. 3. Valence bond resonance structures for the four benzonitriles suggest a grouping into two pairs as far as the ^{14}N quadrupole coupling constants are concerned. Due to the additional double bond structure which can be drawn for para- and ortho-fluoro-benzonitrile, one expects a slightly higher out-of-plane p-electron density at the nitrogen atom for these two molecules (see Table 7) and, as a result, a larger value for the difference between the in-plane and the out-of plane quadrupole coupling constants just as is found from the experiment.

$J_{K_a K_c} - J'_{K'_a K'_c}$	$F - F'$	ν_{exp}	$\Delta\nu_{exp}$	$\Delta\nu_{calc}$	ν_{center}
4 2 2 – 3 2 1	5 – 4	10869.760			10869.594
	4 – 3	10869.159	601	600	
	3 – 2	10869.900	–741	–742	
4 1 3 – 3 1 2	4 – 3	10786.922			10786.884
	3 – 2	10786.867	55	56	
4 2 3 – 3 2 2	5 – 4	9954.464			9954.353
	4 – 3	9953.865	599	600	
	3 – 2	9954.608	–743	–742	
5 0 5 – 4 0 4	6 – 5				11079.203
	5 – 4	11079.224	68	66	
	4 – 3	11079.156			
8 2 6 – 8 2 7	9 – 9				9848.268
	7 – 7	9848.308	101	101	
	8 – 8	9848.207			
10 3 7 – 10 3 8	11 – 11				9401.051
	9 – 9	9401.080	174	174	
	10 – 10	9400.906			
15 5 10 – 15 5 11	16 – 16				10174.766
	14 – 14	10174.816	216	216	
	15 – 15	10174.600			

Table 5. ^{14}N quadrupole hfs multiplets observed for ortho-fluoro-benzonitrile. The frequencies presented here result from decay-fits to the observed transient emission signals as described in the text. The new quadrupole coupling constants reported in Table 3 result from a least squares fit to these splittings. The observed splittings agree with those calculated from the optimized coupling constants within better than 2 kHz, while in the older work [20] discrepancies of 10 kHz and more were typical. (The frequencies are given in MHz.)

In (4) $e q_{210} Q/h$ represents the quadrupole coupling contribution of an electron in an atomic nitrogen p-orbital. Its value is close to -10 MHz [25]. $P_{aa} = 2 \cdot \sum_m C^2_{p_a m}$ etc. represent the p-electron densities at the nitrogen nucleus with the sum running over all doubly occupied molecular orbitals and with $C_{p_a m}$ the LCAO-coefficient of the nitrogen p_a-orbital in the m-th molecular orbital. Equation (4) and the resonance structures sketched in Fig. 3 may now be used for a rough estimate of the coupling constants. For each molecule the nonpolar resonance structure shown in the first row of Fig. 3 will be predominant. In the picture of localized molecular orbitals [26], this resonance structure roughly corresponds to a Slater determinant, in which only four orbitals show nonvanishing contributions in the nitrogen region: the σ-bond, the two double bonds, one in-plane and one perpendicular to the molecular plane, and the lone pair at the nitrogen. With the corresponding LCAO-coefficients presented in Table 6, and the above value of -10 MHz for $e q_{210} Q/h$, we calculate $\chi_{aa} = -5.0$ MHz and $\chi_{bb} = \chi_{cc} = +2.5$ MHz for para-fluoro-benzonitrile and for benzonitrile. This is already in rough agreement with the observed values. The resonance structures shown in Fig. 3 also predict the asymmetry in the CN-bond. The slightest admixture of the polar structures involving a cumulated double bond in the nitrile chain will lead to an increased electron density in the p-orbital perpendicular to the molecular plane. (The corresponding LCAO-coefficients are given in Table 7). Thus, with the admixture of the polar structures, we would also expect the difference $\chi_{cc} - \chi_{bb}$ to become negative and we would expect that this effect should be slightly more pronounced in para-fluoro-benzonitrile than in benzonitrile itself, just because of the additional double bonded structure, which can be drawn for the former. That is indeed what is measured.

The appearent success of the simple minded considerations presented above is contrasted with a "failure" of the much more sophisticated CNDO/2 treatment. As mentioned earlier [27], CNDO/2 wavefunctions predict a higher in-plane than out-of-plane p-density at the nitrogen atom. We note however, that a minimal basis set SCF-calculation carried out already in 1972 by M. Palmer [28], if scaled with our experimental Xaa-value for para-fluoro-benzonitrile (factor: 7.511 MHz/a.u.) gives $\chi_{aa} = -4.171$ MHz, $\chi_{bb} = 2.301$ MHz and $\chi_{cc} = 1.870$ MHz for benzonitrile and $\chi_{aa} = -4.233$ MHz, $\chi_{bb} = +2.344$ MHz, and $\chi_{cc} = +1.890$ MHz for para-fluoro-benzonitrile. Thus the agreement of this calculation with the experimental result is really unexpectedly good, and certainly rather different from the CNDO/2 data.

For the comparison with ortho- and meta-fluoro-benzonitrile as given in Table 3, the quadrupole coupling tensors of the latter had to be transformed from the coordinate system with axes parallel to the molecular principal inertial axes to the principal axes system of the coupling tensors x, y, z. (x-axis closely aligned

	localized orbital	(i, j, k)	$c_{p_i}^2 - (c_{p_j}^2 + c_{p_k}^2)/2$ ⟨x,y,z⟩	⟨y,z,x⟩	⟨z,x,y⟩
— C — N (σ — bond)	$((S_C + P_{xC}) + (S_N + P_{xN}))/2$		1/4	−1/8	−1/8
— C = N (in plane double bond)	$(P_{yC} + P_{yN})/\sqrt{2}$		−1/4	1/2	−1/4
— C — N (out of plane double bond)	$(P_{zC} + P_{zN})/\sqrt{2}$		−1/4	−1/4	1/2
— C — N: (lone pair)	$(S_N + P_{xN})/\sqrt{2}$		1/2	−1/4	−1/4
$2\pi \sum_m (c_{p_i m}^2 - (c_{p_j m}^2 + c_{p_k m}^2)/2) \cdot eQq_{210}/h$			−5 MHz = χ_{xx}	2.5 MHz = χ_{yy}	2.5 MHz = χ_{zz}

Table 6. LCAO-coefficients of localized molecular orbitals which correspond to the triple bonded resonance structures shown in the first row of Fig. 3. With $eq_{210}Q/h = -10$ MHz [25], Eq. (4) of the text then leads to the quadrupole coupling constants presented at the bottom of the Table.

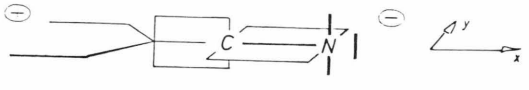

	localized orbital	(i, j, k)	$c_{p_i}^2 - (c_{p_j}^2 + c_{p_k}^2)/2$ ⟨x,y,z⟩	⟨y,z,x⟩	⟨z,x,y⟩
— C — N (σ — bond)	$((S_C + P_{xC}) + (S_N + P_{xN}))/2$		1/4	−1/8	−1/8
— C = N (in plane double bond)	$(P_{yC} + P_{yN})/\sqrt{2}$		−1/4	1/2	−1/4
— C — N: (out of plane lone pair)	P_{zN}		−1/2	−1/2	1
— C — N: (σ lone pair)	$(S_N + P_{xN})/\sqrt{2}$		1/2	−1/4	−1/4
$2\pi \sum_m (c_{p_i m}^2 - (c_{p_j m}^2 + c_{p_k m}^2)/2) \cdot eQq_{210}/h$			0 = χ_{xx}	7.5 MHz = χ_{yy}	−7.5 MHz = χ_{zz}

Table 7. LCAO-coefficients of localized molecular orbitals which correspond to the cumulated double bond in the nitrile chain (polar valence bond structures in Fig. 3). Slight admixture of such structures should lead to an in-plane versus out-of-plane asymmetry in the coupling constants with $\chi_{zz} = \chi_{cc}$, the coupling constant perpendicular to the molecular plane, less positive than the in-plane coupling constant perpendicular to the bond, χ_{yy}.

to the CN-bond, y-axis in the molecular plane, z-axis parallel to the molecular c-axis, i.e. perpendicular to the molecular plane). If the angle θ between the a- and x-axis were known, χ_{xx} and χ_{yy} would follow from the measured values for χ_{aa} and χ_{bb} by solving the system

$$\chi_{aa} = \cos^2(\theta)\,\chi_{xx} + \sin^2(\theta)\,\chi_{yy},$$
$$\chi_{bb} = \sin^2(\theta)\,\chi_{xx} + \cos^2(\theta)\,\chi_{yy}. \quad (5)$$

In our case, the precise value for θ is not yet known from experiment. For the purpose of constructing Table 3 we therefore deliberately assumed that the x-axis of the coupling tensor is exactly aligned to the CN-bond axis and we have calculated the corresponding angle θ from the structures. To account for the ambiguity in this procedure we allowed for a $\pm 1°$ uncertainty in θ. This uncertainty determines the uncertainties of the χ_{xx}- and χ_{yy}-values presented in Table 3. Even with these increased uncertainties, the pairing into benzonitrile and meta-fluoro-benzonitrile with $\Delta\chi \approx 0.3$ MHz on one side and para-fluoro-benzonitrile and ortho-fluoro-benzonitrile with $\Delta\chi \approx 0.4$ MHz on the other side, which is suggested from the valence bond structures shown in Fig. 3, can be infered from the experimental χ-values in Table 3. Simple valence bond theory has thus proved an unexpected predictive strength even for the finer differences in the ^{14}N coupling tensors of the benzonitriles studied here.

Acknowledgements

We would like to thank Dr. B. Kleibömer and Prof. H. Dreizler for critically reading the manuscript. Financial support by Deutsche Forschungsgemeinschaft and Fonds der Deutschen Chemischen Industrie is gratefully acknowledged. The final analysis of the spectra and the CNDO/2 calculations were carried out at the PDP10 computer of the University of Kiel computer center.

Appendix

Since the pioneering work of W. H. Flygare [29, 30] it has been popular among F.T.-microwave spectroscopists to transform the transient molecular emission signals recorded by the averager of the MWFT-spectrometer to the frequency domain by means of a discrete Fourier transformation and then to use the peak frequencies of the so called power spectrum to derive the molecular parameters of interest. Only recently attempts to derive better frequencies by a visual comparison with simulated power spectra have been carried out [31]. This method has been used also in our previous studies of 2- and 4-fluoro-benzonitrile. As is obvious from Table 3, although superior to the direct use of the power spectra, it still leads to unsatisfactory results. The probably most serious drawback of the analysis of the power spectrum, if applied to multiplets, is discussed in the following.

Since the essence of the problem becomes evident already if one examines the more familiar continuous Fourier transform, we will limit our discussion to the latter. Furthermore, for simplicity, we will consider only the case of very short but intense excitation pulses and a time interval, T, between subsequent pulses which is long as compared to the collisional relaxation time, T_2. Also we neglect relaxation due to Doppler dephasing and to mode inhomogeneities in the absorption cell. With these approximations the signal which is detected after superheterodyne down conversion of the microwave emission to an intermediate frequency has the form [32]

$$U_l(t) = -A_l e^{-t/T_2} \cdot \cos(2\pi \nu_l t + \varphi_l). \quad (A.1)$$

A_l = Amplitude of the molecular emission signal. A_l is proportional to the square of the transition dipole matrix element, to the Boltzmann population difference between the lower and the upper level, and to the field-strength of the driving field during pulse excitation. The index l is used for later discrimination of the contributions of different lines.
T_2 = collisional relaxation time. For simplicity the relaxation times will be assumed to be equal for all lines which contribute to the recorded decay.
ν_l = intermediate frequency, i.e. difference between the molecular emission frequency and the local oscillator frequency. ν_l is typically close to 30 MHz in most microwave Fourier transform spectrometers today.
φ_l = phase of the detected signal. It is a sum of a constant term and a term which depends on the i.f. frequency and the delay time, t_d, between the end of the exciting pulse and the start of the sampling. The latter is given by $2\pi\nu_l t_d$. The constant term depends on cable lengths etc. and is the same for all transient emission signals which contribute to the recorded decay. The delay time typically falls into the range of 0.5 μsec to several μsec to allow for pulse echoe decay etc.

We now assume this signal to be periodic with period T. (In a typical experiment T is on the order of 40 μsec corresponding to a 25 kHz repetition rate). Then its continuous Fourier expansion is given as

$$U_l(t) = \frac{a_0}{2} + \sum_n a_{ln} \cdot \cos\left(n \frac{2\pi}{T} t\right) + \sum_n b_{ln} \cdot \sin\left(n \frac{2\pi}{T} t\right) \quad (A.2)$$

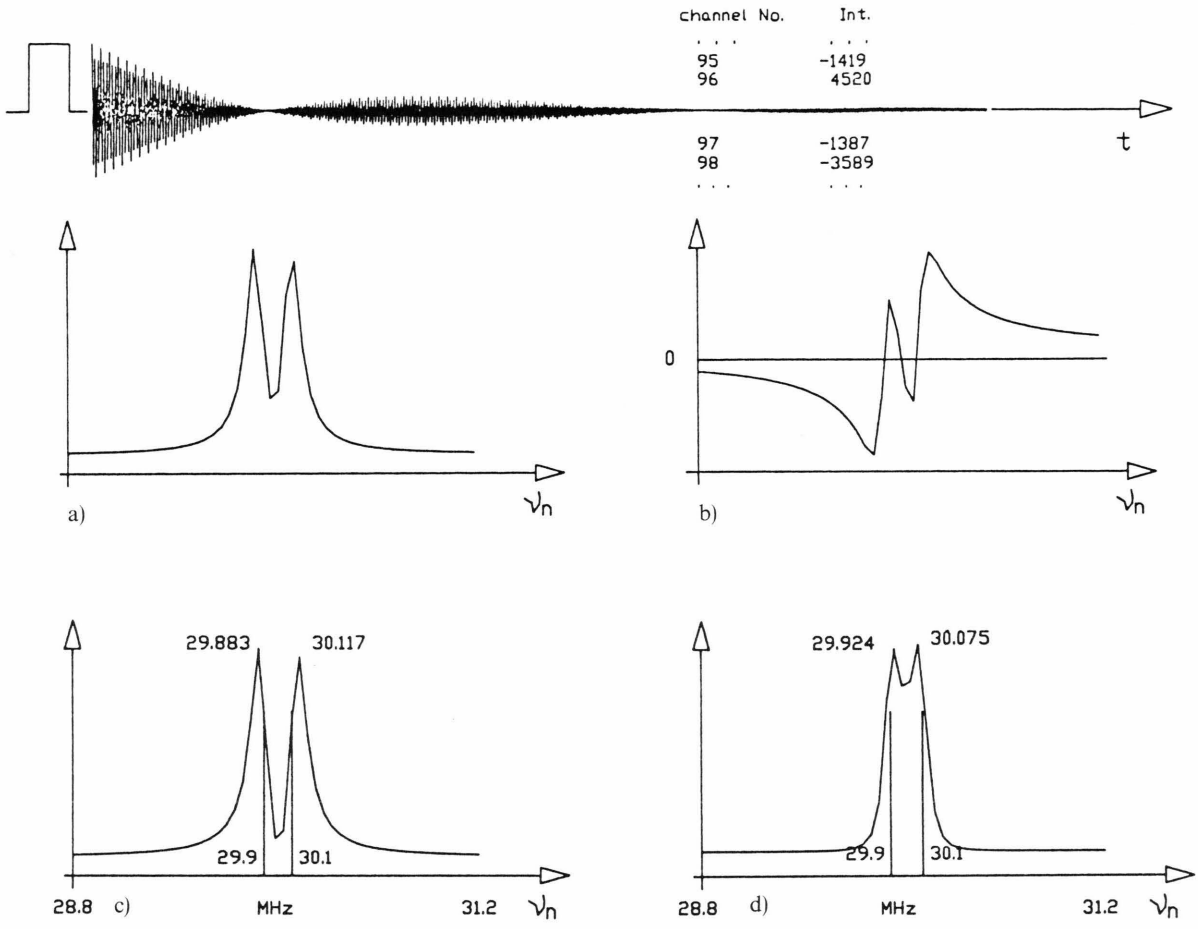

Fig. A.1. In a typical microwave Fourier transform spectrometer the molecular transient emission signal, here assumed to originate from a closely spaced doublet of equal intensity, is heterodyned down to an intermediate frequency close to 30 MHz and is digitized with 10 nsec sampling rate (trace a). – If sampling starts almost immediately after the end of the exciting pulse, the coefficients of the cosine-series, a_{1n}, if plotted against the corresponding frequency, n/T (see text), essentially trace absorption profiles, while the coefficients of the sine-series trace dispersion type profiles (traces b). – Depending on the delay time, absorption type and dispersion type contributions to the a_n-s and b_n-s begin to mix (see (A.3), (A.4), and (A.5) of the text), and the power spectra, $p_n = a_n^2 + b_n^2$, change from too large peak seperations at short delays to too small seperations at longer delays and back again at even longer delays (traces *c* and *d*). – Sampling of 1024 data points with zero filling to a total of 4096 points prior to the discrete F.T. was assumed in these simulations. c) Digitizing assumed to start 0.5 μsec after end of pulse. Peak separation 34 kHz larger than separation of resonance frequencies (200 kHz). – d) Digitizing assumed to start 2.5 μsec after end of pulse. Peak separation 49 kHz smaller than separation of resonance frequencies (200 kHz).

with

$$a_{1n} = \frac{2}{T}\int_0^T U_1(t) \cdot \cos\left(n\frac{2\pi}{T}t\right) \mathrm{d}t\,,$$

$$b_{1n} = \frac{2}{T}\int_0^T U_1(t) \cdot \sin\left(n\frac{2\pi}{T}t\right) \mathrm{d}t\,.$$

For the subsequent discussion it is convenient to split the signal into a cosine-type contribution and into a sine-type contribution. With the cosine addition theorem we get

$$\begin{aligned} U_1(t) &= -\cos(\varphi_1)\, A_1\, e^{-t/T_2} \cos(2\pi\nu_1 t) \\ &\quad + \sin(\varphi_1)\, A_1\, e^{-t/T_2} \sin(2\pi\nu_1 t) \\ &= -\cos(\varphi_1)\, U_{1c}(t) + \sin(\varphi_1)\, U_{1s}(t)\,, \end{aligned} \tag{A.3}$$

where the two subsignals $U_{1c}(t)$ and $U_{1s}(t)$ essentially have the following Fourier components (integrand assumed to be zero at the end of the period; terms including the off resonance denominator $(\nu_1 + n/\tau)^2 +$

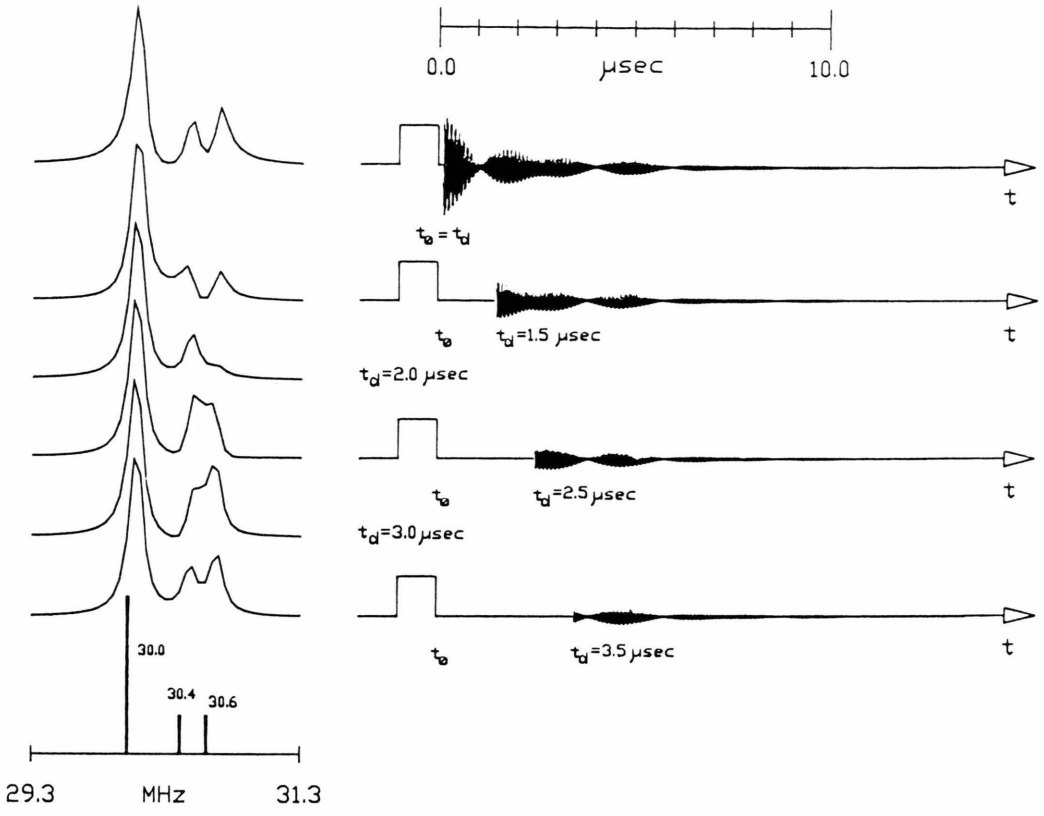

Fig. A.2. Simulation of the delay effect on the power spectrum of a triplet with an amplitude ratio in the transient emission signals of 2:1:1. Here the line shifts are even larger than in the doublet case and the breathing of the peak heights is quite appreciable. In our example the outer satellite at right even vanishes at a delay time close to 2 μsec. – For the computer simulations decays calculated within the short pulse approximation (see text) were subjected to a discrete Fourier transform corresponding to a sampling intervall of 10 nsec and 1 k data points. This accounts for the "corners" in the drawn power spectra. Theo. data: sample interval 10 nsec, 1024 data points, $T_2 = 2.65$ μsec.

$(1/2\pi T_2)^2$ neglected):

$$a_{1cn} = \frac{2}{T}\int_0^T U_{1c}(t)\cdot\cos\left(n\frac{2\pi}{T}t\right)\mathrm{d}t = \frac{A_1}{2\pi T}\frac{(1/2\pi T_2)}{(\nu_1 - n/T)^2 + (1/2\pi T_2)^2},$$

$$b_{1cn} = \frac{2}{T}\int_0^T U_{1c}(t)\cdot\sin\left(n\frac{2\pi}{T}t\right)\mathrm{d}t = \frac{A_1}{2\pi T}\frac{(\nu_1 - n/T)}{(\nu_1 - n/T)^2 + (1/2\pi T_2)^2}$$

and

$$a_{1sn} = \frac{2}{T}\int_0^T U_{1s}(t)\cdot\cos\left(n\frac{2\pi}{T}t\right)\mathrm{d}t = -\frac{A_1}{2\pi T}\frac{(\nu_1 - n/T)}{(\nu_1 - n/T)^2 + (1/2\pi T_2)^2},$$

$$b_{1sn} = \frac{2}{T}\int_0^T U_{1s}(t)\cdot\sin\left(n\frac{2\pi}{T}t\right)\mathrm{d}t = \frac{A_1}{2\pi T}\frac{(1/2\pi T_2)}{(\nu_1 - n/T)^2 + (1/2\pi T_2)^2}, \qquad \text{(A.4)}$$

respectively.

For the special case of a single line with phase angle $\varphi_1 = 0$, the cosine amplitudes, a_{1n}, if plotted against the frequencies n/T, trace an absorption profile:

$$(1/2\pi T_2)/((\nu_1 - n/T)^2 + (1/2\pi T_2)^2),$$

while the sine amplitudes, b_{1n}, trace a dispersion profile:

$$(\nu_1 - n/T)/((\nu_1 - n/T)^2 + (1/2\pi T_2)^2)$$

(see Figure A.1). The power spectrum, which is obtained if the sum $p_n = a_n^2 + b_n^2$ is plotted against the

frequency n/T gives a Lorentzian, centered at the i.f. determined by the difference between the molecular emission frequency and the local oscillator frequency. Its amplitude is proportional to A_1^2 i.e. to the fourth power of the transition dipole matrix element and to the square of the Boltzmann population difference. Its width is determined by the relaxation time, T_2 as given by $\Delta\nu = 1/\pi T_2$ (full width at half height). For such a single line, the profile of the power spectrum is independent of the initial phase of the emission. It is probably this property of the Fourier transform power spectrum, which contributed most to the popularity of this method for the determination of the molecular resonance frequencies.

However for multiplets, where the cosine- and sine-amplitudes in the Fourier expansion each result from a linear superposition of the contributions from the different satellites, the power spectrum is by no means a superposition of Lorentzians and its peak frequencies may differ considerably from the i.f.s corresponding to the true molecular resonance frequencies. As we have noted earlier [11], the far reaching wings of the dispersion-type contributions cause shifts even in cases where the lines appear well resolved. In the computer simulations shown in Figs. A.1 and A.2 we demonstrate the delay time dependence of the overall appearence of a doublet and a triplet respectively.

Note that the intensity fluctuations and frequency shifts in the simulated power spectrum are entirely caused by the delay time dependence of the phases of the different emission signals. Differences in the off-resonance pumping efficiencies, which become important if longer excitation pulses are used, are not accounted for in the simulations.

We note however, that power spectra such as simulated in Figs. A.1 and A.2 can be easily produced with our new microwave Fourier transform Zeeman spectrometer with which well known multiplet splittings can be adjusted by changing the magnetic field.

It was because of the above deficiencies, that J. Haeckel and H. Mäder from our institute have developed the decay-fit routine mentioned above, and it was only recently that we became aware of a similar program developed by D. van Ormondt and coworkers for the analysis of Fourier transform NMR- and ESR-spectra [33].

[1] D. Hübner, M. Stolze, and D. H. Sutter, Z. Naturforsch. **36a,** 332 (1981).
[2] D. Hübner, M. Stolze, and D. H. Sutter, Z. Naturforsch. **37a,** 95 (1982).
[3] A. P. Cox, Y. Kawashima, E. Fliege, and H. Dreizler, Z. Naturforsch. **40a,** 361 (1985).
[4] A. Dutta, A. I. Jaman, D. K. Gosh, and R. N. Nandi, J. Mol. Spectr. **118,** 232 (1986).
[5] G. Bestmann, H. Dreizler, H. Mäder, and U. Andresen, Z. Naturforsch. **35a,** 392 (1980).
[6] G. Bestmann and H. Dreizler, Z. Naturforsch. **37a,** 58 (1981).
[7] G. Bestmann, H. Dreizler, E. Fliege, and W. Stahl, J. Mol. Struct. **97,** 215 (1983).
[8] W. Stahl, G. Bestmann, H. Dreizler, U. Andresen, and R. Schwarz, Rev. Sci. Instrum. **56,** 1759 (1985).
[9] J. Spiekermann and D. H. Sutter, Z. Naturforsch. **40a,** 864 (1985).
[10] Dieter Ziessow, On Line Rechner in der Chemie, Walter de Gruyter, Berlin, New York 1973, p. 110.
[11] W. H. Stolze and D. H. Sutter, Z. Naturforsch. **39a,** 1092 (1984).
[12] Universitätsbibliothek der Christian Albrechts Universität, Olshausenstraße, D-2300 Kiel, West Germany.
[13] J. K. G. Watson, Aspects of Quartic and Sextic Centrifugal Effects on Rotational Energy Levels, in Vibrational Spectra and Structure Vol. 6, Elsevier, Amsterdam 1977.
[14] C. H. Townes and A. L. Schawlow, Microwave Spectroscopy, Dover Publications, Inc., New York 1975, Chapter 6.
[15] See Ref. [13], Eqs. (4–10), (4–52), (6–1), and (6–18).
[16] W. Gordy and R. L. Cook, Microwave Molecular Spectra, Interscience Publishers, New York (1984), p 737.
[17] H. D. Rudolph, Z. Naturforsch. **23a,** 540 (1968).
[18] G. E. Herberich, Z. Naturforsch. **22a,** 593 (1967).
[19] compare too V. Typke, J. Mol. Spectr. **63,** 170 (1976).
[20] Olaf Böttcher and D. H. Sutter, Z. Naturforsch. **41a,** 955 (1986).
[21] Olaf Böttcher and D. H. Sutter, Z. Naturforsch. **41a,** 752 (1986).
[22] E. Fliege, G. Bestmann, R. Schwarz, and H. Dreizler, Z. Naturforsch. **36a,** 1124 (1981).
[23] Kirsten Vormann, Diplom Thesis, Kiel 1987.
[24] J. Mjøberg and S. Ljunggren, Z. Naturforsch. **28a,** 729 (1973).
[25] Ref. [15], Chapter XIV, 13.
[26] W. England, L. S. Salomon, and K. Ruedenberg, Topics Current Chem. **23,** 31 (1971).
[27] compare [21], Table 3.
[28] Michael Palmer, University of Edinburgh, U.K., private communication.
[29] J. C. McGurck, T. G. Schmalz, and W. H. Flygare, Adv. Chem. Phys. **25,** 1 (1974).
[30] J. Ekkers and W. H. Flygare, Rev. Sci. Instrum. **47,** 448 (1976).
[31] E. Fliege and H. Dreizler, Z. Naturforsch. **39a,** 630 (1984).
[32] H. Dreizler, Mol. Phys. **59,** 1 (1986), Eqs. (30) and (40).
[33] H. Barkhuisen, R. de Beer, W. M. J. Boveé, and D. van Ormondt, J. Magnetic Resonance **61,** 465 (1985).
[34] L. Nygaard, I. Bojesen, T. Pedersen, and J. Rastrup-Andersen, J. Mol. Struct. **2,** 209 (1968).
[35] J. Casado, L. Nygaard, and G. O. Sørensen, J. Mol. Struct. **8,** 221 (1971).
[36] D. R. Lide Jr., J. Chem. Phys. **22,** 1577 (1954).
[37] D. G. de Kowalewski, P. Kökeritz, and H. Selén, J. Chem. Phys. **31,** 1438 L (1959).